ATR-IR Flow-Through Cell for Concentration Modulation Excitation Spectroscopy: Diffusion Experiments and Simulations

Atsushi Urakawa, Ronny Wirz, Thomas Bürgi,*,† and Alfons Baiker*

Institute for Chemical and Bioengineering, Swiss Federal Institute of Technology, ETH-Hönggerberg, CH-8093 Zürich, Switzerland

Received: July 10, 2003; In Final Form: September 16, 2003

A new ATR-IR cell was designed, and its performance was characterized by modulation excitation spectroscopy (MES). The new cell allows concentration modulation at relatively high frequency without unnecessary phase delay in the response. The response delay due to convection and diffusion was studied at different flow rates and modulation frequencies by experiments and simulations. The diffusion behavior of a small relatively fast-diffusing molecule, acetonitrile, was compared with that of a large slow-diffusing molecule, hemoglobin, in water. Experimentally, significant differences in their diffusion behavior were observed. The flow and diffusion behavior of the probe molecules was described using two different models, the diffusion layer model and the convection−diffusion model, and the theoretical results were compared with the experiments. The diffusion layer model allows estimating an effective diffusion layer thickness near the surface of the internal reflection element. However, the simulated response is significantly different from the experimental one. On the other hand, the convection−diffusion model describes the flow and diffusion behavior of the solute molecules with high accuracy. This work forms the basis for the investigation of chemical and physical kinetics such as surface reaction and diffusion by MES. It also suggests criteria for appropriate experimental conditions in ATR-IR MES experiments.

Introduction

Attenuated total reflection infrared (ATR-IR) spectroscopy[1] is a powerful tool for the investigation of solid−liquid interfaces. The technique has been applied in a variety of research fields such as for example for the study of model biomembranes,[2,3] environmental chemistry,[4] tribology,[5] diffusion in porous materials,[6] adsorption,[7−9] electrochemistry,[10] high-pressure fluids,[11,12] chiral recognition,[13] and heterogeneous catalysis.[14,15]

With the progress in Fourier transform IR instrumentation, ATR spectroscopy has become well suited to examine chemical kinetics. The step-scan technique allows studying reversible processes with a time resolution on the nanosecond scale. On the other hand, for considerably slower reversible processes (on the second time scale), modulation excitation spectroscopy (MES) has been shown to have significant advantages over the step-scan technique concerning signal-to-noise ratio.[16] The MES technique takes advantage of a digital phase-sensitive detection of the signals induced by a periodic stimulation. The kinetic information of the investigated system is contained in the frequency dependent amplitude of the response and the phase lag between stimulation and response. The transformation from the time- to the phase-domain yields much higher quality spectra and allows a more accurate determination of amplitude and phase lag.[15−17]

Different types of stimulation can be applied to disturb the system by periodically changing an external parameter. Possible external parameters are for example temperature,[18,19] pressure, electric field, light flux,[19] pH,[17] absolute configuration of a probe molecule,[13] or concentration.[15] For the investigation of chemical reactions at interfaces, reactant concentration modulation seems particularly promising. However, for fast concentration modulation at a solid−liquid interface, mass transport has to be considered. This point becomes even more important when multiple internal reflection elements with high geometrical surface area are used in the ATR experiments in order to improve the signal-to-noise ratio. In this case the concentration may vary significantly not only with time but also in space. To correctly extract the kinetics of the chemical step such as adsorption or surface reaction from concentration modulation experiments, mass transport in the ATR cell has to be accounted for.

In this contribution we present an ATR flow-through cell, which allows relatively fast concentration modulation. The performance of the cell is characterized experimentally. Furthermore, the concentration modulation is simulated by applying diffusion layer and convection−diffusion models. This analysis of the transport of dissolved molecules within the ATR flow-through cell forms the basis for the investigation of the kinetics of surface reactions by the combination of ATR-IR and modulation spectroscopy.

Experimental Section

Phase-Sensitive Detection. If a system is perturbed by varying an external parameter periodically, all the species in the system, which are affected by this parameter, will also change periodically at the same frequency as the stimulation or harmonics thereof.[16] It is possible that there is a phase lag between excitation and response. This happens when the time constant of the process giving rise to some signal is on the order

* Authors for correspondence. Phone: +41 32 718 2412. Fax: +41 32 718 2511. E-mail: thomas.burgi@unine.ch. Phone: +41 1 632 3153. Fax: +41 1 632 1163. E-mail: baiker@tech.chem.ethz.ch.

† Current address: Department of Chemistry, University of Neuchâtel, Switzerland.

10.1021/jp0359889 CCC: $25.00
Published on Web 10/31/2003

of the time constant $2\pi/\omega$ of the excitation, where ω is the modulation frequency. At the beginning of the modulation, the system relaxes to a new quasi steady-state around which it is oscillating at frequency ω.[16] In this quasi steady-state, the absorbance variations $A(\tilde{\nu},t)$ are followed by measuring spectra at different times within the modulation period T. This set of spectra, the time-resolved absorbance spectra, are then converted into phase-resolved absorbance spectra by a mathematical treatment, the so-called PSD (phase-sensitive detection) or demodulation, according to eq 1,

$$A_k^{\phi_k^{\mathrm{PSD}}}(\tilde{\nu}) = \frac{2}{T}\int_0^T A(\tilde{\nu},t)\,\sin(k\omega t + \phi_k^{\mathrm{PSD}})\,\mathrm{d}t$$

$$k = 1, 2, \ldots \qquad (1)$$

The integer variable k determines the frequency at which the time dependent signals are demodulated, that is, the fundamental ($k = 1$) of the excitation frequency, first harmonic ($k = 2$), and so on. With one set of time-resolved spectra, eq 1 can be evaluated for different phase settings ϕ_k^{PSD} to obtain different phase-resolved absorbance spectra. The ϕ_k^{PSD} value where $A_k^{\phi_k^{\mathrm{PSD}}}(\tilde{\nu})$ is at the maximum can be directly related to the absolute phase lag, that is, the delay of the response. The maximum amplitude and phase lag reveal how fast a system can respond to a stimulation, and therefore, they can be used to study the kinetics of a system.

Materials

A ZnSe internal reflection element (IRE, 50 × 20 × 2 mm^3, 45°, Komlas) was used for the ATR experiments. Hemoglobin (Fluka, puriss) and acetonitrile (Fluka, puriss pa.) were used as received. As the solvent, filtered water (Milli-Q) was used.

Experimental Setup and Data Acquisition. Infrared spectra were measured on a Bruker IFS 66/S FT-IR spectrometer equipped with a dedicated ATR-IR attachment (Optispec) and a liquid nitrogen cooled MCT detector. All spectra were recorded at a resolution of 4 cm^{-1}. The IRE was fixed within an in house built stainless steel flow cell. The gap between the polished steel surface of the cell and the IRE is about 265 μm and defined by a 30 × 1 mm^2 viton O-ring (Johannsen AG) fit into a precision electroeroded nut of the steel cell. The total volume of the cell is 0.077 mL. The flow-through cell was cooled by means of a thermostat, and the measurements were performed at 20 °C. The flow of liquid was controlled by means of a peristaltic pump (ISMATEC Reglo 100) located behind the cell. Liquid was provided from two separate glass bubble tanks. The flow from the two tanks was determined by two computer-controlled pneumatically actuated three-way Teflon valves (Parker PV-1-2324). Teflon tubing was used throughout.

Design of the New ATR-IR MES Cell. In our earlier ATR-IR MES experiments[13,15] the solution flow from the two bubble tanks was controlled by one three-way Teflon valve above the cell. Only one inlet tube led from the valve to the interior of the cell and to the IRE. This design limited the maximum possible modulation frequency due to back-mixing in the common inlet tube. As a consequence, the stimulation amplitude was significantly attenuated when the modulation frequency was increased.

Therefore, we designed a new cell with two inlet tubes leading to the interior of the cell and coinciding directly above the surface of the ATR-IR IRE (Figure 1). Each of the two inlet tubes is connected through a Teflon valve with a bubble tank, containing the appropriate solution. By closing one of the two

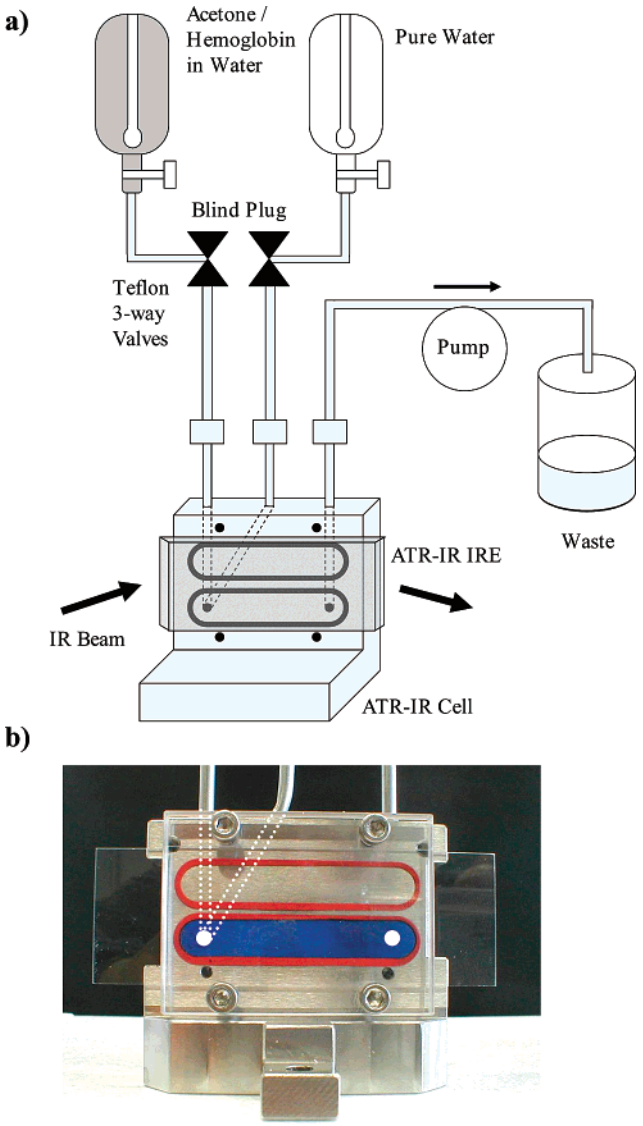

Figure 1. (a) Schematic drawing and description of the cell and experimental setup. (b) Picture of the cell with a glass slide instead of the IRE.

valves, the corresponding solution will stop flowing and the solution of the open valve will pass the cell due to the peristaltic pump situated behind the flow cell. By the simultaneous switching of both valves (one opening, the other closing), the solution flowing through the cell can be changed. This cell design allows increasing the modulation frequency.

The flow behavior in the new cell was examined qualitatively by following a modulation experiment of a transparent and a colored solution. A transparent window was fixed on the flow cell instead of the ATR-IR IRE, and the experiment was monitored. Figure 2 shows nine snapshots of an experiment (flow rate, 1.9 mL/min; modulation frequency, 125 mHz). The time period between the pictures is 1 s. It is clear that the nearly complete exchange of the solute is possible after ~3 s (at 3 and 7 s in Figure 2) even when the relatively high modulation frequency is applied. This possibility of high-frequency modulation plays an important role when kinetics is investigated and a wide range of frequency needs to be examined. One simple criterion for choosing the upper limit of the modulation frequency is taking the capacitive time constant of filling the cell τ ($\tau = V/\phi_V$; ϕ_V, volumetric flow rate; V, volume of the cell) and determining the corresponding frequency f ($f = 1/(2\tau)$;

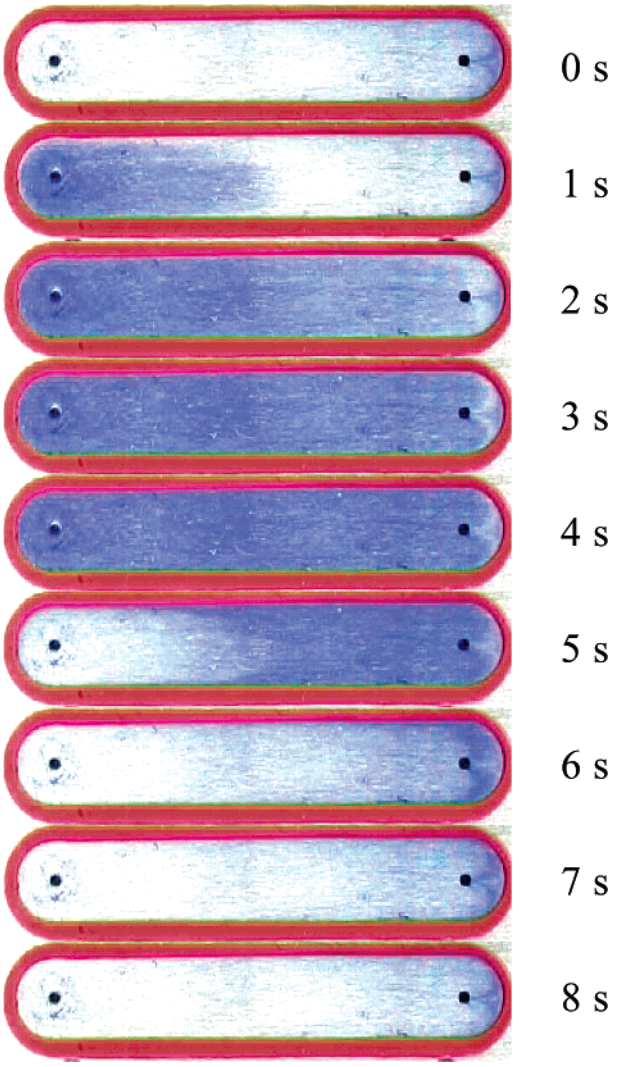

Figure 2. Snapshots of a modulation experiment between water and colored solution: flow rate, 1.9 mL/min; modulation frequency, 125 mHz.

the factor 2 is from the two half-periods). For the conditions mentioned above, τ is 2.4 s and f is 206 mHz. This frequency value is, in principle, the maximum allowed modulation frequency. Since the derivation of the upper limit of the modulation frequency from the capacitive time constant neglects the small velocity and consequently the poor solution exchange near the IRE surface, it is advisable to work with a lower modulation frequency. In general, when an investigation at a higher modulation frequency is required, a larger flow rate is necessary. In case the degree of solute molecules' exchange near the IRE surface is seriously concerned, the treatment of convection and diffusion behavior near the IRE surface by an appropriate model is of great help, as demonstrated in the later sections.

Modulation Experiments. To compare the difference in the convection and diffusion behavior of fast and slow diffusing molecules, several modulation experiments were performed, where an aqueous solution containing both acetonitrile (19 mM for the flow rate 1.2 mL/min and 23 mM for the flow rates 1.5 and 1.9 mL/min) and hemoglobin (15 μM) was modulated against pure water. Two parameters were changed, the flow rate (1.2, 1.5, and 1.9 mL/min) and the modulation frequency (7, 22, and 67 mHz for each flow rate), resulting in nine modulation experiments in total. Per modulation period T, 60 spectra were recorded. Signal averaging was performed over 10, 25, and 50

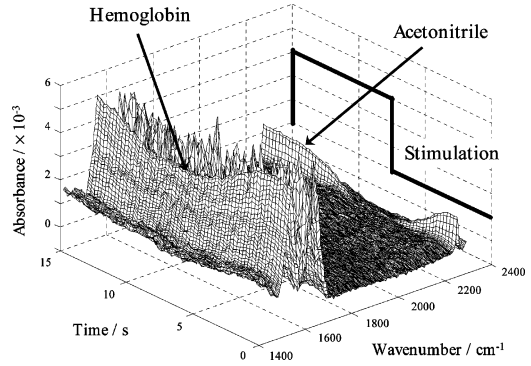

Figure 3. Time-resolved spectra of a modulation experiment: first half period, water; second half period, hemoglobin−acetonitrile aqueous solution; modulation frequency, 67 mHz; flow rate, 1.5 mL/min.

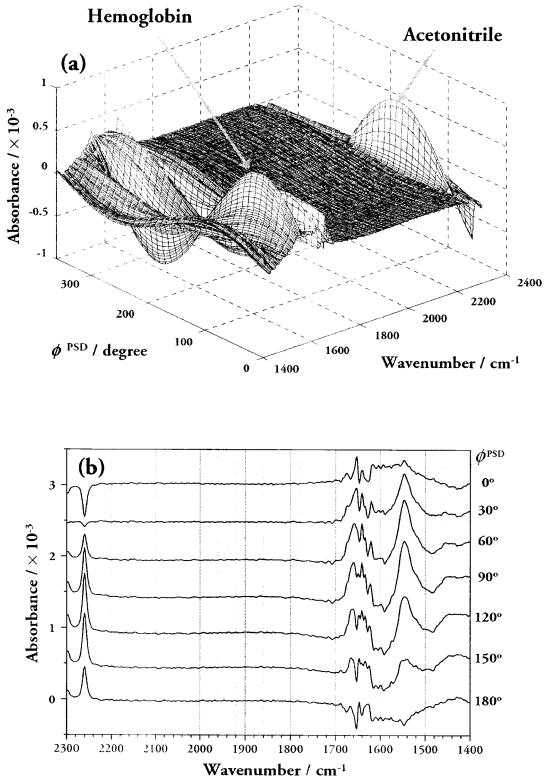

Figure 4. (a) 3-D and (b) 2-D demodulated spectra derived from the time-resolved spectra shown in Figure 3. Absorbance reaches the maximum at ϕ^{PSD} of 64° for hemoglobin (1547 cm^{-1}) and of 126° for acetonitrile (2260 cm^{-1}). The absolute phase lags, that is, the phase delay with respect to the stimulation, of 116° for hemoglobin and 54° for acetonitrile are calculated using the above ϕ^{PSD} values.

periods, and averaging was started after 3, 5, and 10 initial periods at 7, 22, and 67 mHz, respectively, at the flow rates 1.5 and 1.9 mL/min. Signal averaging over 8 periods (after 3 initial periods) was performed at the flow rate of 1.2 mL/min at each frequency.

An example of time-resolved absorbance spectra is shown in Figure 3. The vibrational frequencies at 1547 cm^{-1} for hemoglobin (amide II, δ(N—H)) and at 2260 cm^{-1} for acetonitrile (ν(C≡N)) were chosen as their characteristic bands and analyzed. Clearly, the responses of hemoglobin and acetonitrile are delayed compared to the stimulation. Hemoglobin shows more phase lag than acetonitrile due to its slower diffusion. The phase lag of hemoglobin and acetonitrile signals was analyzed and determined by PSD at the fundamental frequency according to eq 1. The demodulation phase angle ϕ^{PSD} resulting in the maximum absorbance was first determined for hemoglobin and

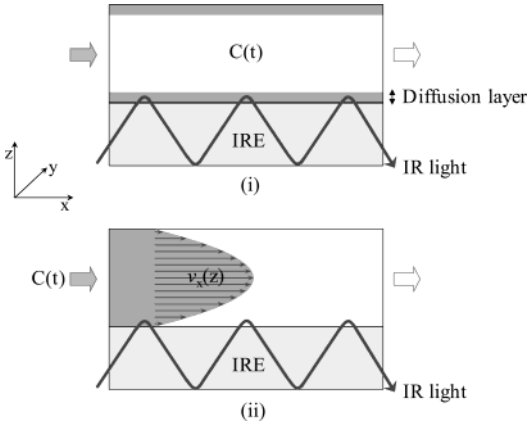

Figure 5. (i) Diffusion layer model and (ii) convection−diffusion model.

acetonitrile (Figure 4), and the absolute phase lag was then calculated. In this example (Figure 4), the absolute phase lags for acetonitrile and hemoglobin were 54° and 116°, respectively. Interestingly, the more intense amide I band (δ(C═O), ~1650 cm^{-1}) of hemoglobin was less pronounced in amplitude compared to the amide II band in the demodulated spectra. This is due to the dilution of water by the presence of hemoglobin molecules near the IRE. The strong water band (~1640 cm^{-1}) overlaps with the amide I band and counteracts its absorbance during the MES experiments (Figure 4b).

Modeling and Simulations

Two models, the diffusion layer model and the convection−diffusion model were applied to describe the diffusion behavior of the solute molecules in the ATR-IR flow-through cell (Figure 5). In the diffusion layer model, a thin diffusion layer near the IRE is assumed to exist due to little fluid velocity near the surface, while, in the convection−diffusion model, no assumption concerning diffusion layer is made. In addition to multidimensional diffusion of the solute molecules, the effect of convection, that is, velocity variance at different positions, is considered. The diffusion coefficients of acetonitrile (1.26×10^{-5} cm^2/s) and hemoglobin (6.9×10^{-7} cm^2/s) were taken from the literature.[20,21] The numerical calculations were carried out by the finite element method implemented in MATLAB[22] and FEMLAB.[23] To examine the steady-state responses of both models (Strictly speaking a steady-state is never reached in MES. Quasi steady-state response is meant here.), 2, 3, and 4 periods were simulated at 7, 22, and 67 mHz modulation frequency, respectively. It was confirmed that the quasi steady-state response is reached within those periods. The last period was analyzed, and the phase lag and the amplitude ratio of the responses were determined by PSD at the fundamental frequency.

Diffusion Layer Model. The following assumptions are made in the diffusion layer model. (1) There is no concentration variation in the *x* and *y* directions (Figure 6). (2) Solute molecules do not adsorb on the IRE. (3) Solute molecules interact only with solvent (water) molecules but do not interact between themselves. The diffusion behavior of molecule A (acetonitrile or hemoglobin) in the layer can then be described by Fick's law, and the mass balance over the layer leads to the well-known diffusion equation.[24,25]

$$\frac{\partial C_A}{\partial t} = D_A \frac{\partial^2 C_A}{\partial z^2} \tag{2}$$

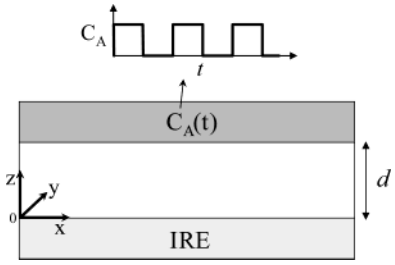

Figure 6. Definition of the diffusion layer model.

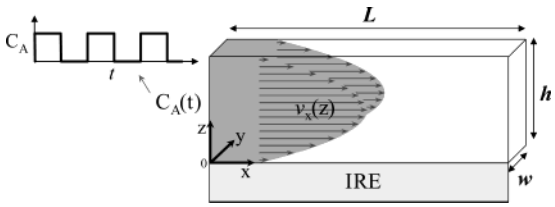

Figure 7. Definition of the convection−diffusion model.

where C_A is the concentration and D_A is the diffusion coefficient of molecule A.

In this diffusion layer model, the flux of molecule A in the layer can be described by Fick's law.

$$J_A = -D_A \frac{\partial C_A}{\partial z} \tag{3}$$

The diffusion equation is solved with the following initial condition and boundary conditions.

Initial condition:

$$0 \le z \le d, \quad t = 0, \quad C_A = 0 \tag{4}$$

Boundary conditions:

$$z = 0, \quad J_A = 0 \tag{5}$$

$$z = d, \quad C_A = SW(t) \tag{6}$$

where J_A is the flux of molecule A and $SW(t)$ represents a square wave. The diffusion layer thickness *d* of 20−30 μm and the same frequency of the square wave concentration modulation as applied in the experiments were considered in the simulations. The concentration change with time at the boundary between solution and the IRE ($z = 0$ in Figure 6) was used to determine the phase lag and amplitude ratio of the responses.

Convection−Diffusion Model. The following assumptions are made in the convection−diffusion model. (1) The solution is a noncompressive Newtonian fluid. (2) The flow is laminar, and the velocity of the solution in the cell has been developed (i.e. does not change with time). (3) There are no concentration variations in the *y* direction and no velocity variations in the *x* and *y* directions (Figure 7). (4) Solute molecules do not adsorb on the IRE. (5) Solute molecules interact only with solvent molecules (same as the diffusion layer model).

The steady-state momentum balance[24,25] yields the following equation for the velocity profile.

$$v_x(z) = \frac{\Delta P(hz - z^2)}{2\eta L} \tag{7}$$

where ΔP is the pressure drop over the cell, η is the viscosity of the solution, and *L*, *w*, and *h* are defined in Figure 7. Now the flow rate can be expressed as

$$\phi_V = w\int_0^h v_x(z)\,dz \tag{8}$$

Therefore, we obtain the following velocity profile expressed by the flow rate instead of the pressure drop.

$$v_x(z) = \frac{6\phi_V}{wh^3}(hz - z^2) \tag{9}$$

Also, the mass balance over the cell leads to the convection−diffusion equation.[24,25]

$$\frac{\partial C_A}{\partial t} = -v_x(z)\frac{\partial C_A}{\partial x} + D_A\left(\frac{\partial^2 C_A}{\partial x^2} + \frac{\partial^2 C_A}{\partial z^2}\right) \tag{10}$$

In this convection−diffusion model, the flux of molecule A can be written as

$$J_A = v_x(z)C_A - D_A\left(\frac{\partial C_A}{\partial x} + \frac{\partial C_A}{\partial z}\right) \tag{11}$$

The diffusion equation is solved with the following initial and boundary conditions.

Initial condition:

$$0 \le x \le L, \quad 0 \le z \le h, \quad t = 0, \quad C_A = 0 \tag{12}$$

Boundary conditions:

$$z = 0, \quad J_A = 0 \quad \text{and} \quad z = h, \quad J_A = 0 \tag{13}$$

$$x = 0, \quad C_A = SW(t) \tag{14}$$

$$x = L, \quad J_A = v_x(z)C_A \tag{15}$$

In simulations, the real cell dimensions were taken as $L = 3.6$ cm (the length between the inlet and outlet), $w = 0.7$ cm, and $h = 265$ μm, and the experimental modulation frequencies were used. Since the concentration change on the IRE surface is relevant to the measurable ATR-IR response, the concentration on the IRE surface was integrated and the change of the latter with time was evaluated by PSD to determine the phase lag and amplitude ratio of the responses.

Results

Comparison between Experiments and the Diffusion Layer Model. Table 1 shows the comparison of the phase lag and the amplitude ratio between the experiments and the diffusion layer model. For both of the solute molecules, in the experiments the phase lag increased at higher modulation frequency and at lower flow rate. The experimental amplitude ratio decreased at higher modulation frequency. The phase lag and the amplitude ratio of the diffusion layer model showed the same trend as the experiments; however, the shapes of the responses of the experiments and the diffusion layer model were not in good agreement (not shown here) and the phase lag was underestimated, significantly for acetonitrile. This indicates that the effect of convection on the phase lag is not negligible.

Both acetonitrile and hemoglobin experience the same convection flow. Therefore, in principle, the difference in their phase lag is due to their different diffusion behavior. Table 2 shows the phase lag difference between acetonitrile and hemoglobin. The agreement becomes better, and roughly, the experimental phase lag difference of the flow rates of 1.9, 1.5, and 1.2 mL/min corresponds to the phase lag difference of the layer thickness of 20, 22, and 25 μm in the diffusion layer model.

TABLE 1. Comparison of Phase Lag and Amplitude Ratio between Experiments and the Diffusion Layer Model[a]

Acetonitrile—Experiments

	flow rate					
	1.9 mL/min		1.5 mL/min		1.2 mL/min	
modulation freq/mHz	PL	AR	PL	AR	PL	AR
7	4	1.00	4	1.00	4	1.00
22	14	0.95	17	0.92	19	0.90
67	41	0.85	54	0.85	63	0.77

Acetonitrile—Diffusion Layer Model

	layer thickness d					
	20 μm		25 μm		30 μm	
modulation freq/mHz	PL	AR	PL	AR	PL	AR
7	1.0	1.00	1.2	1.00	1.5	1.00
22	2.5	1.00	3.2	1.00	4.0	1.00
67	6.2	1.00	8.4	1.00	11.0	0.99

Hemoglobin—Experiments

	flow rate					
	1.9 mL/min		1.5 mL/min		1.2 mL/min	
modulation freq/mHz	PL	AR	PL	AR	PL	AR
7	15	1.00	15	1.00	23	1.00
22	37	0.80	43	0.71	50	0.88
67	100	0.51	116	0.47	122	0.47

Hemoglobin—Diffusion Layer Model

	layer thickness d					
	20 μm		25 μm		30 μm	
modulation freq/mHz	PL	AR	PL	AR	PL	AR
7	8.3	1.00	12.5	1.00	17.7	1.00
22	23.9	0.95	35.3	0.89	47.6	0.83
67	60.4	0.71	80.2	0.55	97.7	0.41

[a] PL, phase lag; AR, amplitude ratio. PL is in degrees and AR is defined as (amplitude)/(amplitude at lowest frequency of the same flow rate).

TABLE 2. Comparison of Phase Lag Difference for Experiments and the Diffusion Layer Model[a]

Experiments

	flow rate		
modulation freq/mHz	1.9 mL/min	1.5 mL/min	1.2 mL/min
7	11	11	19
22	23	26	31
67	59	62	59

Diffusion Layer Model

	layer thickness d			
modulation freq/mHz	20 μm	22 μm	25 μm	30 μm
7	7.3	8.8	11.3	16.2
22	21.4	25.5	32.1	43.6
67	54.2	61.6	71.8	86.7

[a] Phase lag difference is shown in degrees and defined as (phase lag of hemoglobin) − (phase lag of acetonitrile).

Comparison between Experiments and the Convection−Diffusion Model. The convection and diffusion behavior of acetonitrile and hemoglobin in the convection−diffusion model is visualized in Figure 8 for a frequency of 67 mHz and a flow rate of 1.5 mL/min. The difference in their behavior was

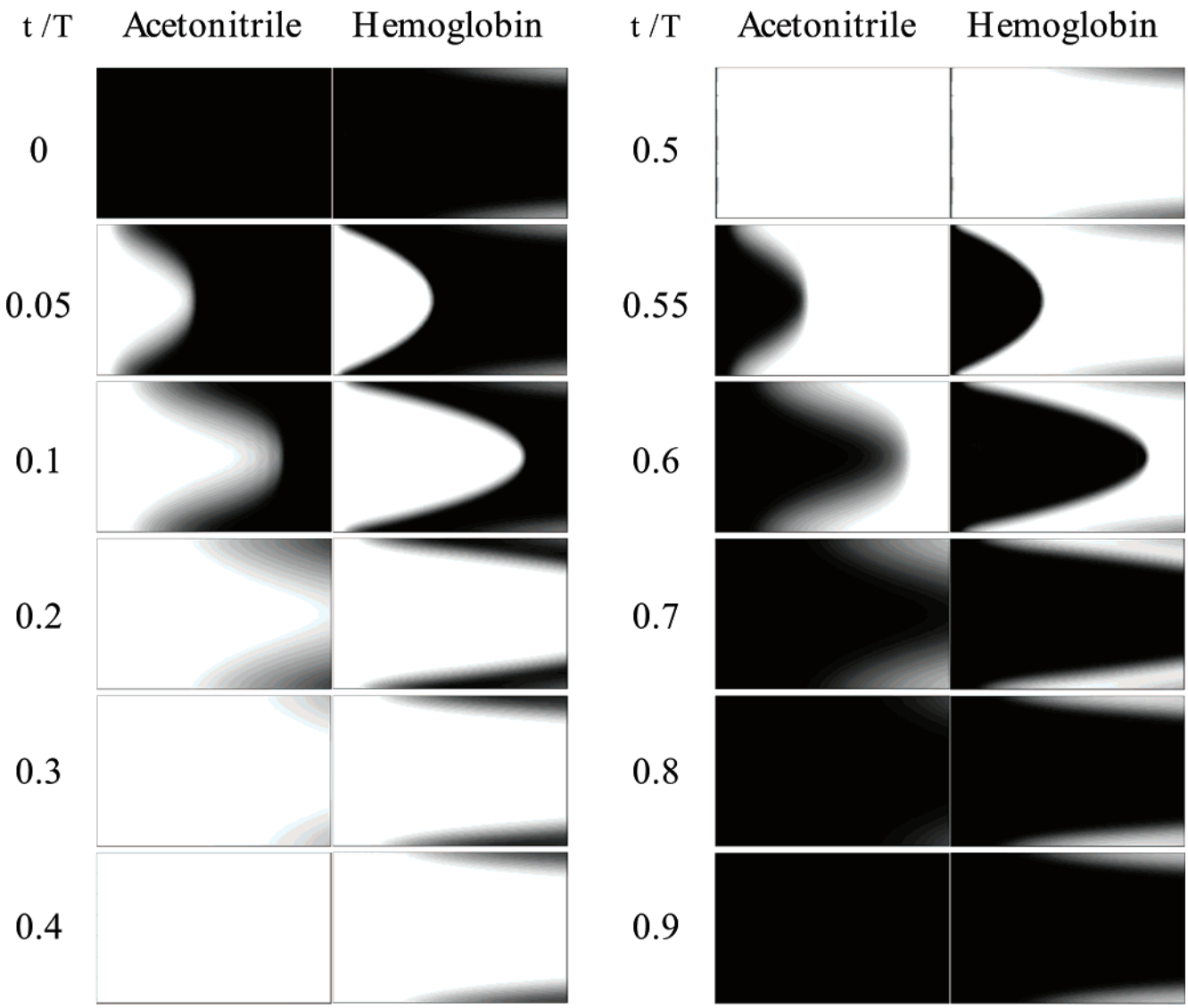

Figure 8. Comparison of the convection and diffusion behavior of acetonitrile and hemoglobin within the convection−diffusion model: modulation frequency, 67 mHz; flow rate, 1.5 mL/min. The displayed region is the cell part in Figure 7. Dark areas represent high concentration of the solute molecules; that is, white represents water. Time is shown relative to the modulation period $T = 14.9$ s.

significant. Obviously, hemoglobin cannot be exchanged completely due to its slow diffusion, and some amount of hemoglobin remains near the IRE at the time of the next stimulation (at $t = 0.5T$). On the other hand, the relatively fast diffusion of acetonitrile makes water−acetonitrile exchange faster. At $t = 0.4T$, almost no acetonitrile is left near the IRE surface.

The hemoglobin and acetonitrile responses of the experiments and the model are compared in Figure 9. Not only the delay but also the slope of the response curves were well described for both hemoglobin and acetonitrile.

Furthermore, the delay and the amplitude of the experimental and simulated responses were analyzed by PSD. Table 3 shows the comparison of the phase lag and the amplitude ratio between the experiments and the convection−diffusion model. The phase lags of both acetonitrile and hemoglobin determined by the convection−diffusion model were in very good agreement with experimental values (mostly within a few degrees). The amplitude ratios also agreed reasonably well.

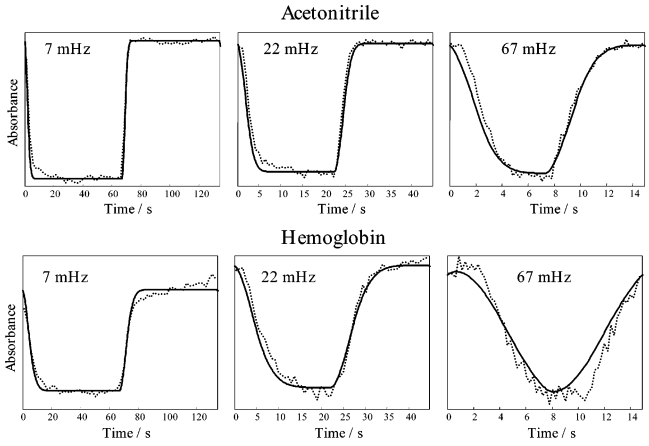

Figure 9. Response comparison between experiments and the convection−diffusion model: flow rate, 1.5 mL/min; solid line, simulated response; doted line, experimental response.

Discussion

Diffusion Experiments. In this study, the diffusion behavior of molecules was experimentally studied by ATR-IR MES. It is possible to detect and quantitatively analyze differences in diffusion behavior of molecules in the liquid phase. PSD allows the accurate determination of phase lag and amplitude ratio.

TABLE 3. Comparison of Phase Lag and Amplitude Ratio between Experiments and the Convection−Diffusion Model[a]

	flow rate											
	1.9 mL/min				1.5 mL/min				1.2 mL/min			
modulation freq/mHz	PL_{exp}	PL_{CD}	AR_{exp}	AR_{CD}	PL_{exp}	PL_{CD}	AR_{exp}	AR_{CD}	PL_{exp}	PL_{CD}	AR_{exp}	AR_{CD}
Acetonitrile												
7	4	5.5	1.00	1.00	4	6.4	1.00	1.00	4	7.4	1.00	1.00
22	14	16	0.95	0.99	17	18.7	0.92	0.99	19	21.8	0.90	0.98
67	41	46.3	0.85	0.91	54	54.3	0.85	0.87	63	63.2	0.77	0.83
Hemoglobin												
7	15	12.4	1.00	1.00	15	14.5	1.00	1.00	23	16.8	1.00	1.00
22	37	36.7	0.80	0.94	43	42.8	0.71	0.92	50	49.4	0.88	0.90
67	100	100.3	0.51	0.57	116	113.1	0.47	0.47	122	125.0	0.47	0.38

[a] PL, phase lag; AR, amplitude ratio; exp, experimental; CD, convection−diffusion model.

This successful application of the technique in a diffusion study will broaden the possibility of ATR to study other diffusion phenomena like diffusion through membranes.

Diffusion Layer Model. First, the diffusion layer model was studied and compared with the experiments. The responses, phase lag, and amplitude ratio did not agree well with the experimental values (Table 1). The phase lag was significantly underestimated, particularly for acetonitrile. The diffusion layer model predicted a maximum phase lag of 11° for acetonitrile within the conditions of this study (layer thickness, 30 μm; modulation frequency, 67 mHz). However, the experiments showed significantly higher phase lags, for example, 63° (flow rate, 1.2 mL/min; modulation frequency, 67 mHz). This observation indicates that the difference in phase lag is mainly due to the neglect of convection effects in the diffusion layer model. Therefore, the difference in phase lag between acetonitrile and hemoglobin was studied to cancel the effect of the convection flow, which is identical for both molecules (Table 2). The phase lag difference with the layer thickness considered in this study showed values in the same range as that of the experiments. Roughly, the experimental phase lag difference at the different flow rates, 1.9, 1.5, and 1.2 mL/min, corresponded to the simulated phase lag difference of the layer thickness, 20, 22, and 25 μm, respectively. This seems intuitively a reasonable result. A high flow rate will raise the fluid velocity near the IRE surface and consequently reduce the thickness of the stagnant diffusion layer. The diffusion layer model allows estimating an "effective" diffusion layer thickness. With the conditions of this work, the effective layer thickness was estimated to be between 20 and 25 μm.

Convection−Diffusion Model. Considering the results of the diffusion-layer model, the inclusion of the convection effect in a model was evidently necessary to describe and understand the experimental absolute phase lag and amplitude ratio. In the convection−diffusion model, the effect of convection flow was explicitly considered. Figure 8 clearly shows the difference between acetonitrile and hemoglobin concerning the exchange of molecules and the diffusion behavior. The small molecule, acetonitrile, can diffuse very fast in both x and z directions, which makes the exchange of molecules near the IRE surface faster. On the contrary, the large molecule, hemoglobin, diffuses very slowly and stays near the IRE surface. The slow diffusion of hemoglobin is also apparent from the clear laminar flow profile in Figure 8, whereas the one of the acetonitrile is smeared out due to diffusion. This difference in their diffusion behavior is also well-seen at $t = 0.8$ s. Near the IRE where the ATR signal is generated, the dark area (i.e. high concentration of the solute molecules) has propagated almost until the end of the cell for acetonitrile; in contrast, for hemoglobin, only about 25% of the IRE surface is in contact with the dark area.

The agreement in the responses, phase lag, and amplitude ratio between the experiments and the simulation corroborates the validity of the model (Figure 9, Table 3). The assumptions made in the model seem appropriate, and the model could describe the diffusion behavior of molecules with high accuracy. However, careful inspection of the responses indicates possibilities for further improvement of the experiments. First, the experimental signal does not reach a constant value as fast as the simulated one, for example, 7 and 22 mHz in Figure 9. This can be due to the fact that the inlet of a solution, that is, the boundary, in the convection−diffusion model is not the same as the one of the real cell. With the real cell, a solution flows in all directions and the solution is more stagnant on the left side of the inlet and especially on the right side of the outlet, as seen in Figure 2. The slow exchange of fluids in those regions by a convective flow could be responsible for the observed small discrepancies between experiment and simulation. Second, an almost constant absorbance is observed at the beginning of solution exchange, as prominently seen at $t = 0-1$ and 7.5−8 s for acetonitrile and $t = 0-3$ and 7.5−11 s for hemoglobin in Figure 9. This may also be due to the design of the cell inlet. In the experiments, solute molecules have to travel the distance $h = 265$ μm to be detected upon stimulation, while they are immediately seen on the IRE surface in the applied convection−diffusion model. This traveling distance h may be responsible for the initial constant absorbance upon solution exchange. Part of this distance close to the IRE has to be overcome by diffusion, which is the reason the effect is more pronounced for hemoglobin. Although the effect of the inlet, outlet, and cell geometry on the deviations in the phase lag and amplitude ratio between experiment and the convection−diffusion model considered in this work is not large, there is some space for further improvement to attain more ideal responses. Another interesting observation is the gradual absorbance increase for hemoglobin during stimulation at 7 and 22 mHz (Figure 9). In contrast, the absorbance remains constant for acetonitrile at the same stimulation frequency. This can be due to the reversible slow adsorption/desorption process of hemoglobin on the IRE surface during stimulation.

This study implies that phase lag and amplitude ratio vary remarkably depending on the diffusion behavior of solute molecules and flow rate. When complete or nearly complete exchange of solute molecules is desired, one can use the diffusion layer model, estimate an effective diffusion layer thickness, and try to reduce the thickness by optimizing conditions. Alternatively, via the convection−diffusion model, concentration changes near the IRE surface during modulation can be studied and the degree of modulation on the surface itself can be determined. Another positive aspect of the latter model is that one can also estimate the phase lag due to both diffusion

and, especially, convection. The model helps us to understand those effects on phase lag and amplitude ratio observed experimentally. This is advantageous, since complete exchange of solute molecules is not required in order to analyze the kinetics of processes. Although numerical calculations for the convection−diffusion model can be computationally demanding, it is worthwhile to investigate phase lag and amplitude ratio by the model and determine which factor is playing the prominent role in the delay of the response. Before a kinetic study by ATR-IR MES using concentration modulation, the effects of convection and diffusion should carefully be considered in order to correctly examine a chemical and physical system of interest.

Conclusion

An ATR-IR cell suitable for dynamic measurements was designed, and its behavior was characterized by modulation excitation spectroscopy. The new cell decreases the problematic back-mixing of solutions and allows concentration modulation at much higher frequency without unnecessary phase delay in the response. The delay of the response in the new cell could be traced to the effects of convection, that is, the velocity of the liquid flow in the cell, and diffusion of probe molecules.

The diffusion behavior of molecules in the cell was investigated using two tracer compounds having significantly different diffusivity, acetonitrile and hemoglobin in water. Experimentally, remarkable differences in their diffusion behavior were observed by ATR-IR MES. First, the diffusion behavior was modeled by a diffusion layer model, where a thin stagnant diffusion layer was assumed near the IRE surface. The cancellation of the influence of the convection flow in the diffusion layer model allowed us to estimate the effective diffusion layer thickness of 20−25 μm for the conditions applied in this study. With the convection−diffusion model, on the other hand, the effect of convection was explicitly included and it was possible to model and describe the flow and diffusion behavior of the probe molecules with good accuracy. The simulations showed that, at high modulation frequency, a large slow-diffusing molecule, such as hemoglobin, cannot be exchanged easily during ATR-IR MES experiments and a detectable amount of the molecule stays near the IRE throughout the modulation period with small concentration variations. On the other hand, a small fast-diffusing molecule, such as acetonitrile, can be completely exchanged near the IRE with relative ease.

This work provides the grounds for determining the phase lag originating from the chemical and physical systems by knowing the phase lag caused by the effect of convection and diffusion. Thus, it forms the basis for the investigation of the kinetics of processes, such as adsorption−desorption on a surface, surface reactions, and diffusion through porous media. Furthermore, it gives criteria for the appropriate modulation frequency and flow rate in ATR-IR MES experiments.

Acknowledgment. We thank Prof. U. P. Fringeli and Dr. D. Baurecht, Institute of Physical Chemistry, University of Vienna, for helpful discussions and practical support and P. Steiner and H.-P. Schläpfer for building the cell. Financial support from the Swiss National Science Foundation and the Foundation Claude and Giuliana is kindly acknowledged.

References and Notes

(1) Harrick, N. J. *Internal reflection spectroscopy*; Interscience: New York, 1967.
(2) Fringeli, U. P. In situ infrared attenuated total reflection membrane spectroscopy. In *Internal reflection spectroscopy, theory and applications*; F. M. Mirabella, J., Ed.; Dekker: New York, 1992; p 255.
(3) Wenzel, P.; Fringeli, M.; Goette, J.; Fringeli, U. P. *Langmuir* **1994**, *10*, 4253.
(4) Hug, S.; Sulzberger, B. *Langmuir* **1994**, *10*, 3587.
(5) Piras, F. M.; Rossi, A.; Spencer, N. D. *Langmuir* **2002**, *18*, 6606.
(6) Rivera, D.; Harris, J. M. *Anal. Chem.* **2001**, *73*, 411.
(7) Degenhardt, J.; McQuillan, A. J. *Langmuir* **1999**, *15*, 4595.
(8) Zippel, E.; Kellner, R.; Krebs, M.; Breiter, M. W. *J. Electroanal. Chem.* **1992**, *330*, 521.
(9) Ferri, D.; Bürgi, T. *J. Am. Chem. Soc.* **2001**, *123*, 12074.
(10) Osawa, M. *Bull. Chem. Soc. Jpn.* **1997**, *70*, 2861.
(11) Wolf, U.; Leiberich, R.; Seeba, J. *Catal. Today* **1999**, *49*, 411.
(12) Schneider, M.; Grunwaldt, J.-D.; Bürgi, T.; Baiker, A. *Rev. Sci. Instrum.* **2003**, *74*, 4121.
(13) Wirz, R.; Bürgi, T.; Baiker, A. *Langmuir* **2003**, *19*, 785.
(14) Moser, W. R.; Marshik-Guerts, B. J.; Okrasinski, S. J. *J. Mol. Catal., A: Chem.* **1999**, *143*, 57.
(15) Bürgi, T.; Baiker, A. *J. Phys. Chem. B* **2002**, *106*, 10649.
(16) Baurecht, D.; Fringeli, U. P. *Rev. Sci. Instrum.* **2001**, *72*, 3782.
(17) Fringeli, U. P.; Baurecht, D.; Günthard, H. H. Biophysical Infrared Modulation Spectroscopy. In *Infrared and Raman Spectroscopy of Biological Materials*; Gremlich, H. U., Yan, B., Eds.; Dekker: New York/Basel, 2000; p 143.
(18) Baurecht, D.; Porth, I.; Fringeli, U. P. *Vib. Spectrosc.* **2002**, *30*, 85.
(19) Müller, M.; Buchet, R.; Fringeli, U. P. *J. Phys. Chem.* **1996**, *100*, 10810.
(20) *CRC Handbook of Chemistry and Physics*, 3rd electronic ed.; CRC Press Inc.: 2003.
(21) Tanford, C. *Physical Chemistry of Macromolecules*; Wiley: New York, 1963.
(22) The MathWorks. MATLAB ver. 6.5.
(23) COMSOL. FEMLAB ver. 2.3.
(24) Beek, W. J.; Muttzall, K. M. K. *Transport Phenomena*; Wiley−Interscience: 1975.
(25) Bird, R. B.; Stewart, W. E.; Lightfoot, E. N. *Transport Phenomena*; John Wiley & Sons: 1960.